

Ultrasensitive, universal single-ion nanodetector

Namita Narendra* and Tillmann Kubis*

Elmore Family School of Electrical and Computer Engineering, Purdue University, West Lafayette, Indiana 47907, United States

E-mail: nnarendr@purdue.edu; tkubis@purdue.edu

Abstract

In this paper, a carbon nanotube (CNT) based single-ion detector is proposed and its performance is evaluated with atomistic quantum transport models. The sensor can detect any ion type without molecule-specific functionalization and allows for continuous real-time ion monitoring. A single ion temporarily changes the operating principle of the sensor's CNT field-effect transistor into a resonant tunneling diode. The concrete device example of this paper showed a source-drain current increase of 5 orders of magnitude induced by a single ion.

Single-ion sensing is essential for a range of applications such as the detection of picomolar levels of biomarkers,^{1–3} the detection of traces of heavy metal ions,^{4,5} or nanoscale quantum applications.^{6,7} Scaling down of the ion sensors to sizes comparable to those of molecules has increased sensitivity and made single-ion sensing feasible.^{8–11} State-of-the-art ion nanosensors, such as nanopores^{12–14} and nanowire transistors,^{15,16} have drawn attention due to their label-free real-time sensing capabilities. However, most of these nanosensors require functionalization for specific ion types.^{17–19} Universal ion sensors that are sufficiently sensitive to detect individual ions have yet to be developed.

In this paper, we propose a concept for an ultrasensitive single-ion detector based on carbon nanotube field-effect transistors (CNT FETs). CNTs have traditionally been pro-

posed as chemical sensors by detecting change in conductivity through surface reaction and adsorption.^{20–22} In contrast, we use CNTs as ion channels that confine ion propagation to the 1D CNT interior but allow for continuous propagation of the ion without physisorption or chemisorption of the ion on the CNT surface. In consequence, the CNT ion sensors allow for non-destructive ion sensing. Any ion that enters the CNT will be detected, since no ion-specific functionalization is needed. The CNT sensor can detect ions of both polarities and is compatible with nanodevice typical signal-improving electronics.²³

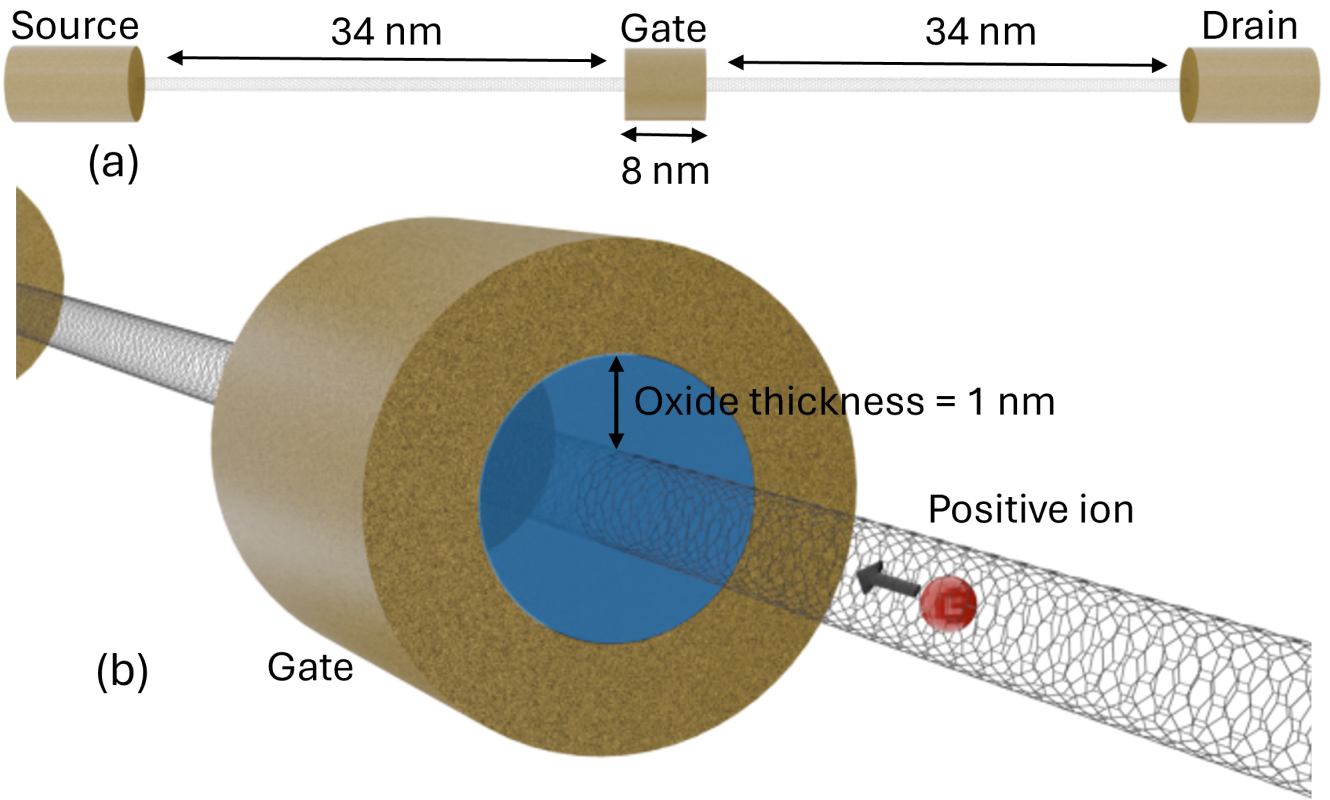


Figure 1: Schematic of the CNT based single-ion detector: The side view in (a) shows the dimensions of the specific CNT FET structure considered in the main text. Ions within the CNT channel get detected when they enter the gate region as illustrated in (b).

The core of the proposed device is a semiconducting CNT FET structure^{24,25} in Figure 1 that detects ions that propagate through the CNT channel. Once the ion is sufficiently close to the gate region, it transforms the CNT FET into a resonant tunneling diode (RTD):²⁶ The attractive charge of the ion yields discrete quantum dot states in the CNT. Electrons or

holes that have to pass the barrier in the gate region can use these quantum dot states for resonance tunneling through the barrier. This process changes the source-drain current (I_{ds}) of the CNT device by several orders of magnitude when the gate voltage is tuned to maximize the resonant tunneling. For positive (negative) ions, the CNT FET will be configured for n-type (p-type) operation. The channel gate electrode is a gate-all-around electrode²⁴ for maximal ion sensitivity. Back gate electrodes²⁷ are used to control the effective doping density and doping type. Electric fields at the entry of the CNT can funnel ions into the CNT channel²⁸ if needed.

All electronic transport results presented in this paper are solved in the Nonequilibrium Green's Function (NEGF) implementation of the nanodevice simulation tool NEMO5.²⁹ Electrons are discretized in the atomic representation of Ref. 30. Electronic energies in the Dyson and Keldysh equations are self-adaptively discretized to reliably resolve ion-induced electronic resonances and band edges of the CNT-FET.³¹ Charge self-consistency is ensured by iterating the NEGF equations with the nonlinear Poisson equation.³² The Poisson equation is solved on the finite element mesh of libMesh³³ which was adapted to the respective atomic geometry of the CNT and the ion in all three dimensions. Source and drain contacts are treated as Ohmic, while the gate contact is included as a Dirichlet boundary condition with cylindrical symmetry around the CNT. The charge distribution of all electrons, including deep-lying valence band electrons and electrons of partly filled conduction bands, is solved explicitly within the NEGF approach of Ref. 34. In this way, the electrostatic screening of valence band electrons that do not take part in transport is explicitly included for every voltage and ion location. This lifts the requirement of defining highly anisotropic dielectric screening constants within and perpendicular to the CNT surface. Correspondingly, the dielectric constant in the Poisson equation is set to the one of vacuum. Ions are represented as point charges in the Poisson equation that interact with CNT electrons only electrostatically.

The sensor concept is exemplified with a n-type semiconducting (11,0) CNT FET (di-

ameter of 8.7 \AA) at room temperature. 76 nm of the CNT FET are explicitly solved with NEGF, while the remaining homogeneous CNT is covered with open boundary conditions. An 8 nm long cylindrical gate is centered around a 8 nm long intrinsic CNT section that is surrounded by 34 nm long source and drain regions with an n-type doping density of $1.5 \times 10^{19} \text{ cm}^{-3}$. This doping density corresponds to an electron density of $0.16 e^-/\text{nm}$, which is within the experimentally measured range.³⁵ The drain-source voltage (V_{ds}) is set to 0.05 V.

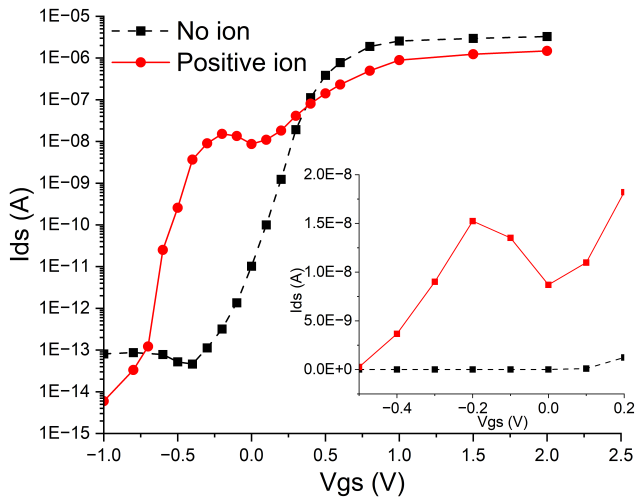


Figure 2: Drain-source current density of the single ion detector of Fig. 1 with (red solid lines) and without (black dashed lines) a positive ion in the CNT channel under the gate. An ion with a charge of 1 e under the gate switches the device's performance from a standard FET characteristics to the one of a resonant tunneling diode. The negative differential resistance of the diode is highlighted in the linear-scale inset. The sensor's highest sensitivity is around the diode's current density peak at a gate bias of -0.2 V in the considered device.

Figure 2 shows the drain current, I_{ds} , as a function of the gate voltage (V_{gs}) for two device scenarios: No ion in the CNT FET (dashed black line) and a positive ion in the center of the gate region (solid red line). Comparison of the I-V characteristics demonstrates the positive ion in the CNT channel effectively transforms the CNT FET into a CNT-based RTD: The I-V characteristic of the CNT FET with the ion has a pronounced negative differential resistance (NDR) right after the current maximum at -0.2 V gate voltage (highlighted by the inset in Fig. 2). The positive ion induces a quantum well with resonant energy levels, as illustrated

in detail in Fig. 3:

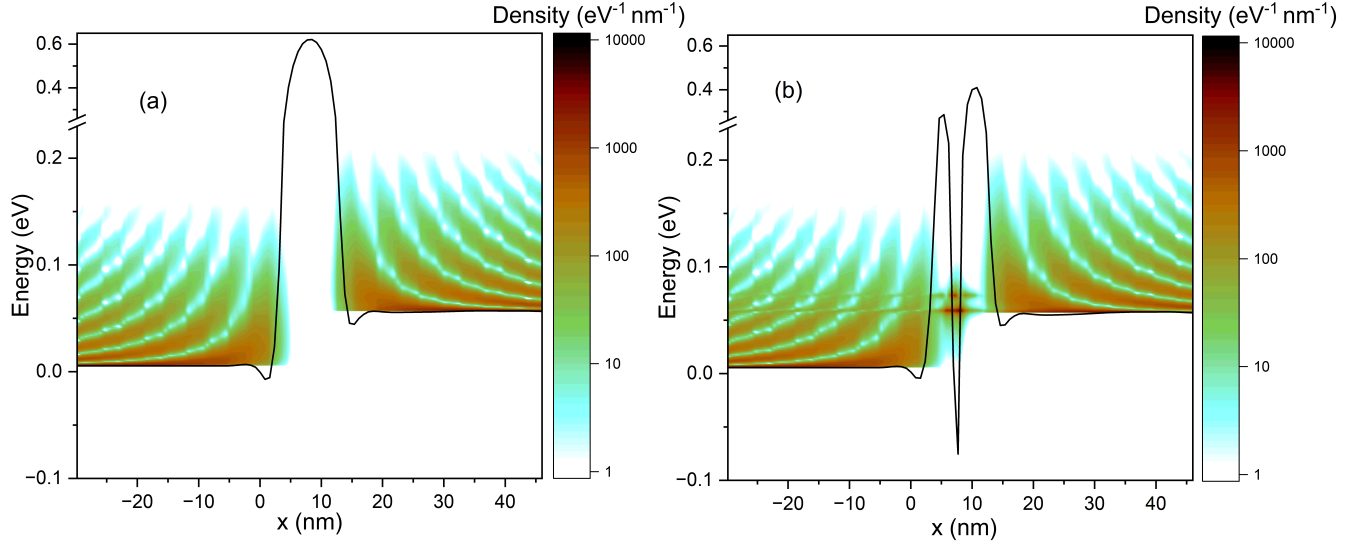


Figure 3: Conduction band energy (line) and contour graph of the spatially and energy resolved electron density along the surface of the CNT of Fig. 1 at the resonant gate voltage of -0.2 V for (a) no ion in the CNT and (b) a positive ion centered in the CNT channel under the gate at 7.5 nm. The gate extends from 4.2 nm to 12.2 nm.

Figure 3 shows the contour graphs of the position and energy resolved electron density for the case with (a) no ion and with (b) a positive ion in the CNT channel at an applied gate voltage of -0.2 V. The solid line in both graphs indicates the respective effective conduction band edge as a function of position. The conduction band edge in Fig. 3(a) resembles the typical potential profile of n-type FETs with intrinsic gate regions.³⁶ At the given V_{gs} of -0.2 V, the CNT FET is effectively turned off and electrons are completely reflected at the gate barrier. This causes the interference pattern of the energy and position resolved density in Fig. 3(a). In contrast, the positive ion induces a quantum well in the middle of the gate barrier which yields a RTD-typical double barrier profile.²⁶ The maxima of the spectral function in the gate region (between 4.2 nm and 12.2 nm) in Fig. 3(b) correspond to the quantum confined states of that induced quantum well. For the shown V_{gs} of -0.2 V, the first quantum confined state aligns with the conduction band edge of the CNT source side (at 50 meV). This alignment allows electrons to resonantly tunnel through the gate region and thereby to maintain I_{ds} of nearly 5 orders of magnitude larger than the current in the

ion-free CNT FET case. The linewidths of the involved quantum confined states determine the height and width of the RTD IV resonance.²⁶

In consequence, the presented single ion sensor operates with the highest sensitivity when its gate voltage is set to the resonant voltage of the CNT RTD (here at $V_{gs} = -0.2$ V): When no ion is in the channel, the sensor is turned off and I_{ds} vanishes. With an ion in the gate region, the sensor turns into a CNT RTD at its resonance condition i.e., it maintains a high I_{ds} .

Figure 4 shows I_{ds} as a function of the ion position along the CNT axis. As can be seen from the graph, the ion induces a source-drain current only when it is within the gate region (marked by vertical lines).

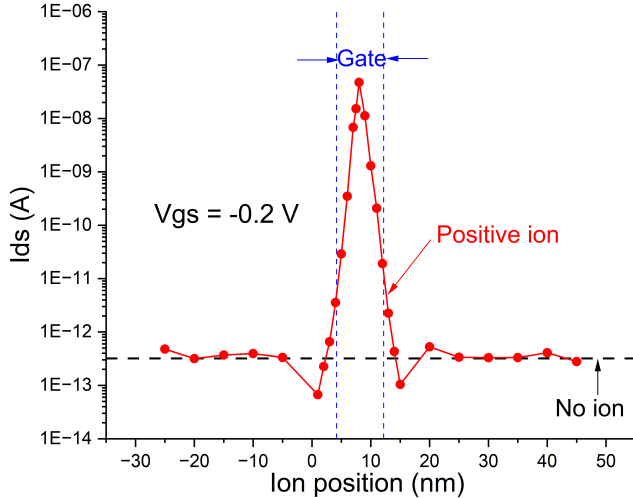


Figure 4: Source-drain current density of the CNT sensor of Fig. 1 as a function of the ion position centered in the channel along the CNT axis for a gate voltage of -0.2 V. The solid line is only meant to guide the eye. The dashed horizontal line shows the drain current without an ion in the channel. The dashed vertical lines indicate the gate region.

The ion in the center of the gate region induces quantum confined states that wrap around the complete CNT circumference as can be seen in Fig. 5 for the first quantum confined state at the energy of $E = 0.059$ eV.

In summary, this paper introduces and quantitatively assesses a new type of CNT based single-ion detector. Unlike conventional CNT sensors, the proposed device does not need functionalization and can serve as a universal ion detector. The sensor behaves like a CNT

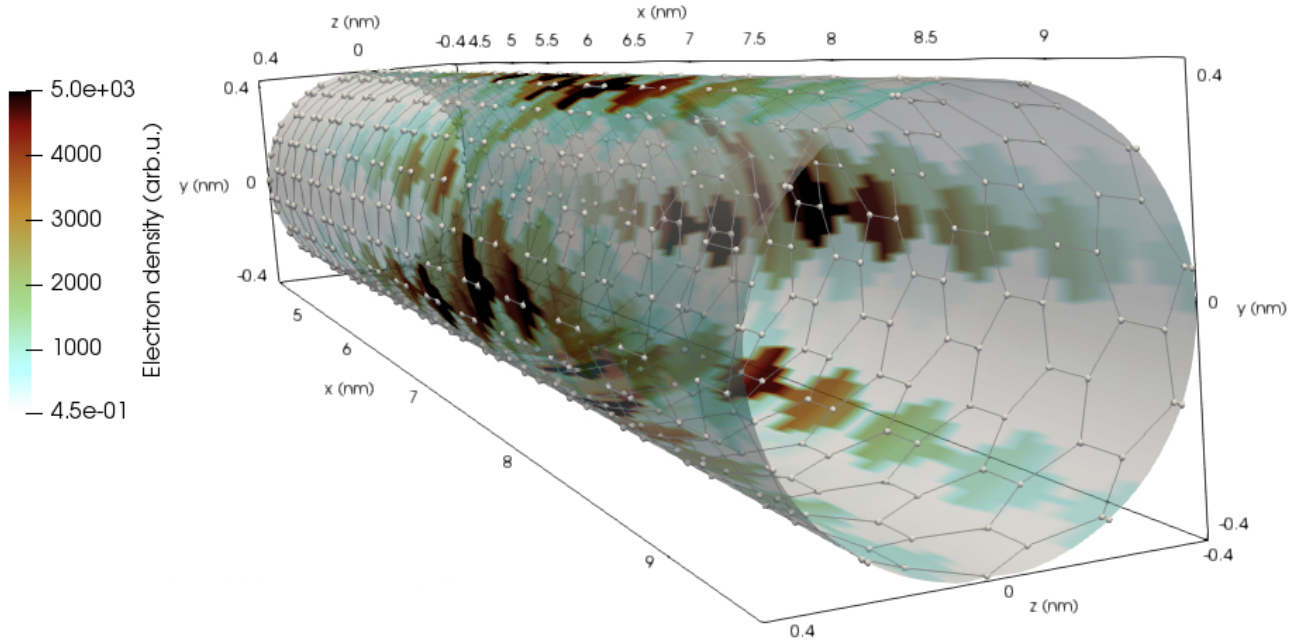


Figure 5: Contour graph of the electron density of the first ion-induced quantum confined state at $E = 0.059$ eV of Fig. 3(b) projected on the CNT surface. The positive ion is placed at the CNT center axis at $x=7.5$ nm.

FET when no ion is in the CNT channel. The Coulomb potential of a single ion in the CNT channel under the gate region changes the electronic device behavior from FET into RTD. Once the ion leaves the gate region the sensor returns to the FET behavior. The concrete sensor example of this work was predicted to show a signal-to-noise ratio of 5 orders of magnitude. Such an ultrasensitive single-ion sensor can enable breakthroughs in biomedical, environmental, and quantum applications.

Acknowledgement

Computational resources were provided by the Negishi Research Computing Cluster (RCAC) at Purdue University. The authors also thank Manas Pratap for his assistance in creating the figures and improving the visual quality of this work.

References

- (1) Visser, E. W.; Yan, J.; van IJzendoorn, L. J.; Prins, M. W. Continuous biomarker monitoring by particle mobility sensing with single molecule resolution. *Nature communications* **2018**, *9*, 2541.
- (2) Raveendran, M.; Lee, A. J.; Sharma, R.; Wälti, C.; Actis, P. Rational design of DNA nanostructures for single molecule biosensing. *Nature communications* **2020**, *11*, 4384.
- (3) Zou, J.; Bai, H.; Zhang, L.; Shen, Y.; Yang, C.; Zhuang, W.; Hu, J.; Yao, Y.; Hu, W. W. Ion-sensitive field effect transistor biosensors for biomarker detection: current progress and challenges. *Journal of Materials Chemistry B* **2024**, *12*, 8523–8542.
- (4) Shtenberg, G.; Massad-Ivanir, N.; Segal, E. Detection of trace heavy metal ions in water by nanostructured porous Si biosensors. *Analyst* **2015**, *140*, 4507–4514.
- (5) Si, L.; Wu, Q.; Jin, Y.; Wang, Z. Research progress in the detection of trace heavy metal ions in food samples. *Frontiers in chemistry* **2024**, *12*, 1423666.
- (6) Yoo, J.; Kim, H.; Kim, H.; Kim, Y.; Choi, T. Trapped-ion based nanoscale quantum sensing. *Nano Convergence* **2025**, *12*, 12.
- (7) Bonus, F.; Knapp, C.; Valahu, C.; Mironiuc, M.; Weidt, S.; Hensinger, W. Ultrasensitive single-ion electrometry in a magnetic field gradient. *Nature Physics* **2025**, 1–7.
- (8) Nakajima, A. Application of single-electron transistor to biomolecule and ion sensors. *Applied Sciences* **2016**, *6*, 94.
- (9) Gooding, J. J.; Gaus, K. Single-molecule sensors: challenges and opportunities for quantitative analysis. *Angewandte Chemie International Edition* **2016**, *55*, 11354–11366.
- (10) Baaske, M. D.; Vollmer, F. Optical observation of single atomic ions interacting with plasmonic nanorods in aqueous solution. *Nature Photonics* **2016**, *10*, 733–739.

(11) Bhardwaj, A.; Radha, B.; Varma, M.; Keerthi, A.; others Microtomy-fabricated two-dimensional nano-slits enable single molecule biosensing. *Nanoscale* **2025**, *17*, 18605–18613.

(12) Miles, B. N.; Ivanov, A. P.; Wilson, K. A.; Doğan, F.; Japrung, D.; Edel, J. B. Single molecule sensing with solid-state nanopores: novel materials, methods, and applications. *Chemical Society Reviews* **2013**, *42*, 15–28.

(13) Roozbahani, G. M.; Chen, X.; Zhang, Y.; Wang, L.; Guan, X. Nanopore detection of metal ions: Current status and future directions. *Small Methods* **2020**, *4*, 2000266.

(14) Graf, M.; Lihter, M.; Altus, D.; Marion, S.; Radenovic, A. Transverse detection of DNA using a MoS₂ nanopore. *Nano letters* **2019**, *19*, 9075–9083.

(15) Hu, Q.; Chen, S.; Solomon, P.; Zhang, Z. Ion sensing with single charge resolution using sub-10-nm electrical double layer-gated silicon nanowire transistors. *Science Advances* **2021**, *7*, eabj6711.

(16) Li, J.; He, G.; Ueno, H.; Jia, C.; Noji, H.; Qi, C.; Guo, X. Direct real-time detection of single proteins using silicon nanowire-based electrical circuits. *Nanoscale* **2016**, *8*, 16172–16176.

(17) Ahoulou, S.; Perret, E.; Nedelec, J.-M. Functionalization and characterization of silicon nanowires for sensing applications: A review. *Nanomaterials* **2021**, *11*, 999.

(18) Ren, R.; Zhang, Y.; Nadappuram, B. P.; Akpinar, B.; Klenerman, D.; Ivanov, A. P.; Edel, J. B.; Korchev, Y. Nanopore extended field-effect transistor for selective single-molecule biosensing. *Nature communications* **2017**, *8*, 586.

(19) Yao, X.; Zhang, Y.; Jin, W.; Hu, Y.; Cui, Y. Carbon nanotube field-effect transistor-based chemical and biological sensors. *Sensors* **2021**, *21*, 995.

(20) Schroeder, V.; Savagatrup, S.; He, M.; Lin, S.; Swager, T. M. Carbon nanotube chemical sensors. *Chemical reviews* **2018**, *119*, 599–663.

(21) Norizan, M. N.; Moklis, M. H.; Demon, S. Z. N.; Halim, N. A.; Samsuri, A.; Mohamad, I. S.; Knight, V. F.; Abdullah, N. Carbon nanotubes: Functionalisation and their application in chemical sensors. *RSC advances* **2020**, *10*, 43704–43732.

(22) Acharya, R.; Patil, T. V.; Dutta, S. D.; Lee, J.; Ganguly, K.; Kim, H.; Randhawa, A.; Lim, K.-T. Single-Walled Carbon Nanotube-Based Optical Nano/Biosensors for Biomedical Applications: Role in Bioimaging, Disease Diagnosis, and Biomarkers Detection. *Advanced Materials Technologies* **2024**, *9*, 2400279.

(23) Shim, J. W.; Gu, L. Q. Stochastic sensing on a modular chip containing a single-ion channel. *Analytical chemistry* **2007**, *79*, 2207–2213.

(24) Franklin, A. D.; Koswatta, S. O.; Farmer, D. B.; Smith, J. T.; Gignac, L.; Breslin, C. M.; Han, S.-J.; Tulevski, G. S.; Miyazoe, H.; Haensch, W.; others Carbon nanotube complementary wrap-gate transistors. *Nano letters* **2013**, *13*, 2490–2495.

(25) Lin, Y.; Cao, Y.; Ding, S.; Zhang, P.; Xu, L.; Liu, C.; Hu, Q.; Jin, C.; Peng, L.-M.; Zhang, Z. Scaling aligned carbon nanotube transistors to a sub-10 nm node. *Nature Electronics* **2023**, *6*, 506–515.

(26) Bowen, R. C.; Klimeck, G.; Lake, R. K.; Frensel, W. R.; Moise, T. Quantitative simulation of a resonant tunneling diode. *Journal of applied physics* **1997**, *81*, 3207–3213.

(27) Chiu, H.-Y.; Safron, N.; Passlack, M.; Chao, T.-A.; Su, S.-K.; Mao, P.-S.; Chou, C.-H.; Huang, H.-Y.; Wu, G.-Z.; Chen, C.-W.; others Overcoming the Leakage and Contact Resistance Challenges in Highly Scaled PMOS and NMOS Carbon Nanotube Transistors. *Nano letters* **2025**, *25*, 3981–3988.

(28) Su, J.; Guo, H. Control of unidirectional transport of single-file water molecules through carbon nanotubes in an electric field. *ACS nano* **2011**, *5*, 351–359.

(29) Steiger, S.; Povolotskyi, M.; Park, H.-H.; Kubis, T.; Klimeck, G. NEMO5: A parallel multiscale nanoelectronics modeling tool. *IEEE Transactions on Nanotechnology* **2011**, *10*, 1464–1474.

(30) Neophytou, N.; Ahmed, S.; Klimeck, G. Non-equilibrium Green's function (NEGF) simulation of metallic carbon nanotubes including vacancy defects. *Journal of Computational Electronics* **2007**, *6*, 317–320.

(31) Eiseman, P. R. Adaptive grid generation. *Computer Methods in Applied Mechanics and Engineering* **1987**, *64*, 321–376.

(32) Birner, S.; Zibold, T.; Andlauer, T.; Kubis, T.; Sabathil, M.; Trellakis, A.; Vogl, P. Nextnano: general purpose 3-D simulations. *IEEE Transactions on Electron Devices* **2007**, *54*, 2137–2142.

(33) Kirk, B. S.; Peterson, J. W.; Stogner, R. H.; Carey, G. F. libMesh: a C++ library for parallel adaptive mesh refinement/coarsening simulations. *Engineering with Computers* **2006**, *22*, 237–254.

(34) Chu, Y.; Sarangapani, P.; Charles, J.; Klimeck, G.; Kubis, T. Explicit screening full band quantum transport model for semiconductor nanodevices. *Journal of applied physics* **2018**, *123*.

(35) Lee, C.-S.; Pop, E.; Franklin, A.; Haensch, W.; Wong, H. A compact virtual-source model for carbon nanotube field-effect transistors in the sub-10-nm regime—Part I: Intrinsic elements. *IEEE Trans. Electron Devices*

(36) Dang, T.; Anghel, L.; Leveugle, R. Cntfet basics and simulation. International Confer-

ence on Design and Test of Integrated Systems in Nanoscale Technology, 2006. DTIS 2006. 2006; pp 28–33.

TOC Graphic

